Mechanical characterization and modeling of the stress flow of a cemented tungsten carbide over wide ranges of temperatures and strain rates

C Francart

Mechanical characterization and modeling of the stress flow of a cemented tungsten carbide over wide ranges of temperatures and strain rates

C. Francart

Université de Grenoble-Alpes, Laboratoire 3SR, 38400 Saint-Martin-d'Hères, France

Abstract

Cemented carbide tungsten are materials which are broadly used in the design of cutting and machining tools. However, in the open literature, very few experimental data allow to grasp the strain behavior of cemented tungsten carbide under uniaxial loading. This study aims to provide reliable true strain vs true stress curves of a WC-10%Co K25 cemented tungsten alloy from 0.0001 /s to 6000 /s in compression and shear-compression and from room temperature to 743 K (above the temperature of phase transformation of the Cobalt). The mechanical behavior of the stress flow is commented and elements of explanation are suggested through the consideration of microstructural information found in the literature and SEM pictures of fracture profiles. A modeling of the mechanical behavior is also proposed with the calibration of the Johnson-Cook models for the stress flow behavior for industrial application in classic Finite Element Software such as ABAQUS® or LS-Dyna®.

1. Introduction

Cemented tungsten carbides, often simply called tungsten carbine through misuse of language, are materials composed generally of a WC ceramic matrix and of a binder (around 10%) which can generally be Cobalt or Nickel. This kind of materials are nearly exclusively used in cutting and machining tools of all kinds of materials (metals, composites, wood …) due to their very high hardness (around 90 HRA) and their low adiabatic heating for the high strain rates encountered in such high-speed machining. Other kind of applications of cemented tungsten carbides can be enounced such as mining tools or ball bearings.

However, even if these materials present exceptional wear resistance [1, 2] and very high mechanical properties, their important brittleness might leads to severe failure of the tools if used above their limits. The investigation of the mechanical behavior of such materials at high strain rate needs therefore to be performed to allow better designs of machining tools. However, very few study concerning the mechanical characterization of cemented tungsten carbide exists in the literature and most of them are only based on values of Transverse Rupture Strength obtained through three-point bending tests [3-5], on Fracture Toughness [2-4, 6, 7] or on hardness tests [2, 3, 5, 6]. Studies on the strain vs stress behavior are very rare and generally under bending loading [3, 8] and therefore an important lack of data under uniaxial loading which may help to grasp the strain behavior of such materials can be reported and more especially at high strain rates.

In this paper, the mechanical behavior of a K25 cemented tungsten carbide (WC-10%Co close to the Pobedit Russian grade) is thoroughly studied in compression and shear-compression. Experimental tests have been carried out over wide ranges of strain rates (from 0.0001 /s to 6000 /s) and temperatures (from room temperature to 743 K) in order to investigate the mechanical response of cemented tungsten carbide under different kind of loadings. A microstructural study of the failure profiles has also been carried out through SEM pictures to examine the failure causes. These experimental data have been next used to calibrate Johnson-Cook model for the stress [9] behavior which can be used in Finite Element Software like Abaqus® or LS-Dyna® for part design.

2. Material

The grade of cemented carbide tungsten studied in this work is K25 from the manufacturer Ultra-met®. The Ultra-met® sub-grade is UF110 which consists into a material composed of 10% Co (binder) and a matrix of 90% WC (weight percentage) with ultra-fine grain size (between 1 and 5 µm). Its average

hardness is around 92.3 HRA with a density of $\rho = 14425\ kg.m^{-3}$ and a specific heat of $C_p = 280\ J.kg^{-1}.K^{-1}$.

This material is usually used as cutting materials in the industry for the design of drill bit, cutting disk or milling tools. Such machining tools are used for all kind of materials such as steels, non-ferrous or even non-metallic materials.

This material will be assumed as a biphasic material consisting into a Hexagonal Close Packed (HCP) metallic Cobalt phase ($P_{Co} = 10\%$) and an orthorhombic ceramic WC phase ($P_{WC} = 90\%$). It can be noted that the Cobalt undergoes a phase transformation starting from 690 K from HCP structure to a FCC structure [5]. During the strain hardening of the material, the mechanisms of plastic deformation (e.g. dislocations slip) occur quasi exclusively in the metallic HCP phase [11]. Indeed, the ceramic orthorhombic WC phase stays in its elastic domain of deformation [11]. Due to these phenomena, the Taylor-Quinney coefficient χ cannot be considered as it is usually done for fully plastic metals. In this study, a value of χ is computed from the assumed values of $\chi_{Co} = 1$ and $\chi_{WC} = 0$ pondered with their respective densities (Eq. 1). The computed value of χ is $\chi = 0.0595$, leading to a limited adiabatic heating of the material at high strain rates (using $\rho_{WC} = 15630\ kg.m^{-3}$ and $\rho_{Co} = 8900\ kg.m^{-3}$). The elastic modulus of the material has been measured using the wave method and evaluated at $E = 630\ GPa$ and the Poisson ratio at $\nu = 0.24$. The increase of temperature during an adiabatic plastic deformation is then computed using Eq. 2.

$$\chi = \frac{\chi_{Co}\rho_{Co}P_{Co} + \chi_{WC}\rho_{WC}P_{WC}}{\rho_{Co}P_{Co} + \rho_{WC}P_{WC}} \quad (1)$$

$$\Delta T = \frac{\chi}{\rho C_p}\int \sigma d\varepsilon_p \quad (2)$$

3. Experimental method

a. Quasi-static condition

The tests in quasi-static conditions have been carried out using a uniaxial INSTRON testing machine with harder and larger tungsten carbide platens. The load has been measured with a 100kN force cell and the displacement with a calibrated LVDT. No irreversible deformation has been observed on the platens after the tests. All sample ends have been lubricated with petroleum jelly before the tests. Compression and shear-compression [12] tests have been performed using the geometries respectively presented in the Figure 1.a and 1.b. Compliance correction of the machine has to be thoroughly investigated before the data processing since most of the measured displacement corresponds to the deformation of the testing tools.

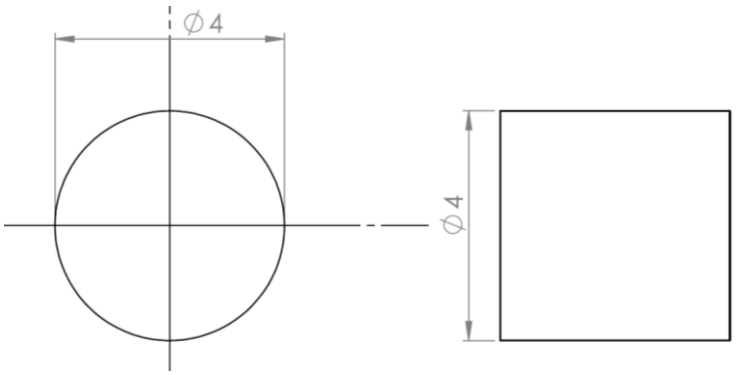

(a)

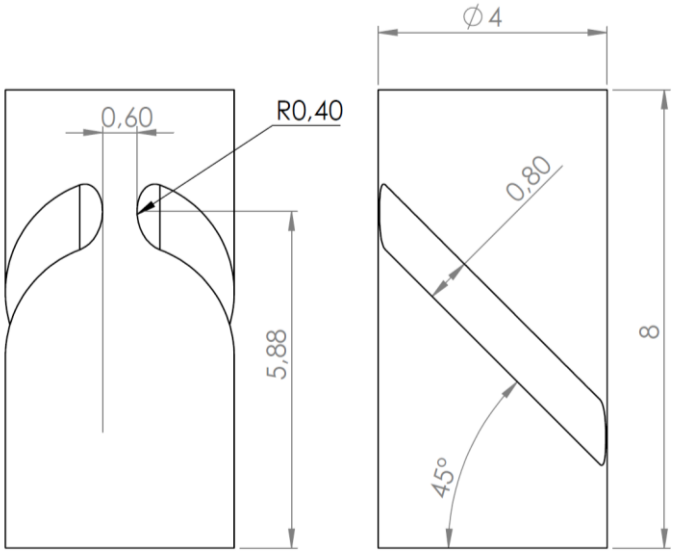

(b)

Figure 1 - Technical drawing of the (a) compression sample and (b) shear-compression sample used in this study

The processing of the data of the shear-compression tests have been performed using Eqs. 3 and 4 to get the true equivalent strain ε_{eq} and the true stress σ from the shortening of the specimen d and the load F. The parameters k_i are obtained through numerical simulations using ABAQUS/Explicit® [12] and are linked to the geometry of the shear-compression sample used (see Table 1). The determination of the k_i parameters has been performed with the least square fitting that can be seen in Figures 2.a and 2.b. It can be noted that, in this study, the elastic part cannot be neglected and the determination equivalent strain requires two linear expressions valid for small values of plastic strain (with d_y the shortening of the specimen at the yield point of the deformation process). The value of k_1 is determined to coincide with the elastic behavior (using $E = 630\ GPa$ and $\nu = 0.24$) computed in the numerical simulation.

$$\begin{cases} \varepsilon_{eq} = k_1 d & if\ d < d_y \\ \varepsilon_{eq} = k_2 d + k_3 & if\ d \geq d_y \end{cases} \quad (3)$$

$$\sigma = k_4\left(1 - k_5 \varepsilon_{eq}\right)F \quad (4)$$

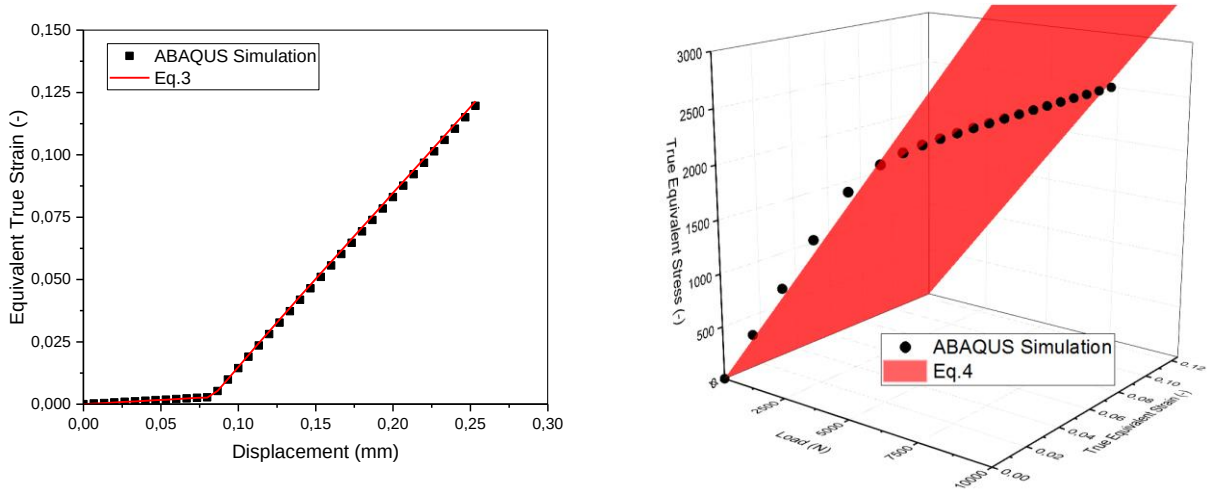

(a) (b)

Figure 2 - Determination of the k_i parameters linked to the (a) true equivalent strain and to the (b) true equivalent stress through least square fitting from the ABAQUS simulation data

Table 1 - Values of the parameters required for the processing of the shear-compression tests

k_1	k_2	k_3	k_4	k_5
0.03415	0.6864	-0.0531	0.3709	0.4049

b. Dynamic condition

The tests in dynamic conditions have been carried out using a Split Hopkinson Pressure Bar setup [13, 14] (SHPB) (see Table 2). As for the quasi-static tests, tungsten carbide platens have been set next to the steel bar ends in order to avoid punching damage. The platens have been designed in order to avoid any impedance mismatch with the steel bars. The elastic deformations of the bars have been recorded using two full bridges of strain gages linked to a signal magnifier and finally to an oscilloscope. The output signal has been amplified 20 times for the compression tests and 100 times for the shear-compression tests in order to get reliable data. All sample ends have been lubricated with petroleum jelly before the tests. The shortening of the specimen d and the average have been obtained using the processing software David® (with punching correction [15]). The parameters k_i used in dynamic conditions are the same than in quasi-static conditions. However, it can be noted that the value of k_3 might be adjust to ensure a good connection between the elastic and plastic domains of the final curve (k_3 pilots the translation the plastic domain).

Table 2 - Characteristics of the SHPB setup

Material	Input Bar	Output Bar	Strikers
Steel	Ø = 20 mm L = 1.8 m	Ø = 20 mm L = 1.8 m	Ø = 20 mm L = 0.4 m

4. Experimental results

a. Compression condition

The true strain-true stress curves from the quasi-static tests in compression are shown in Figure 3.a. It can be seen that the experimental procedure applied allows to obtain reproducible data for five consecutive tests which can therefore be considered as representative of the mechanical behavior of the material. The compression tests have also been carried out in dynamical conditions (Figure 3.b) for which the level of stress is slightly higher than in quasi-static condition (see Figure 3.d). The yield stress in quasi-static condition is around $\sigma_{yQS} = 2400\,MPa$ and in dynamic condition around $\sigma_{yD} = 2750\,MPa$. Some quasi-static compression tests at elevated temperature have also been carried out up to 743 K and a clear thermal softening can be observed (Figure 3.c). The isothermal condition found in Figure 3.d has been obtained through the consideration of the thermal sensitivity which can be computed thanks to the data in Figure 3.c.

In all cases, the range of true strain is low (around 0.025) before failure. In these conditions, the stage IV (asymptotic behavior of the stress at high plastic strain) of structural hardening cannot be seen and only the stage III is observable as it can be seen with the hardening rate on Figure 5.d (highly dependent to temperature and strain rate) [16].

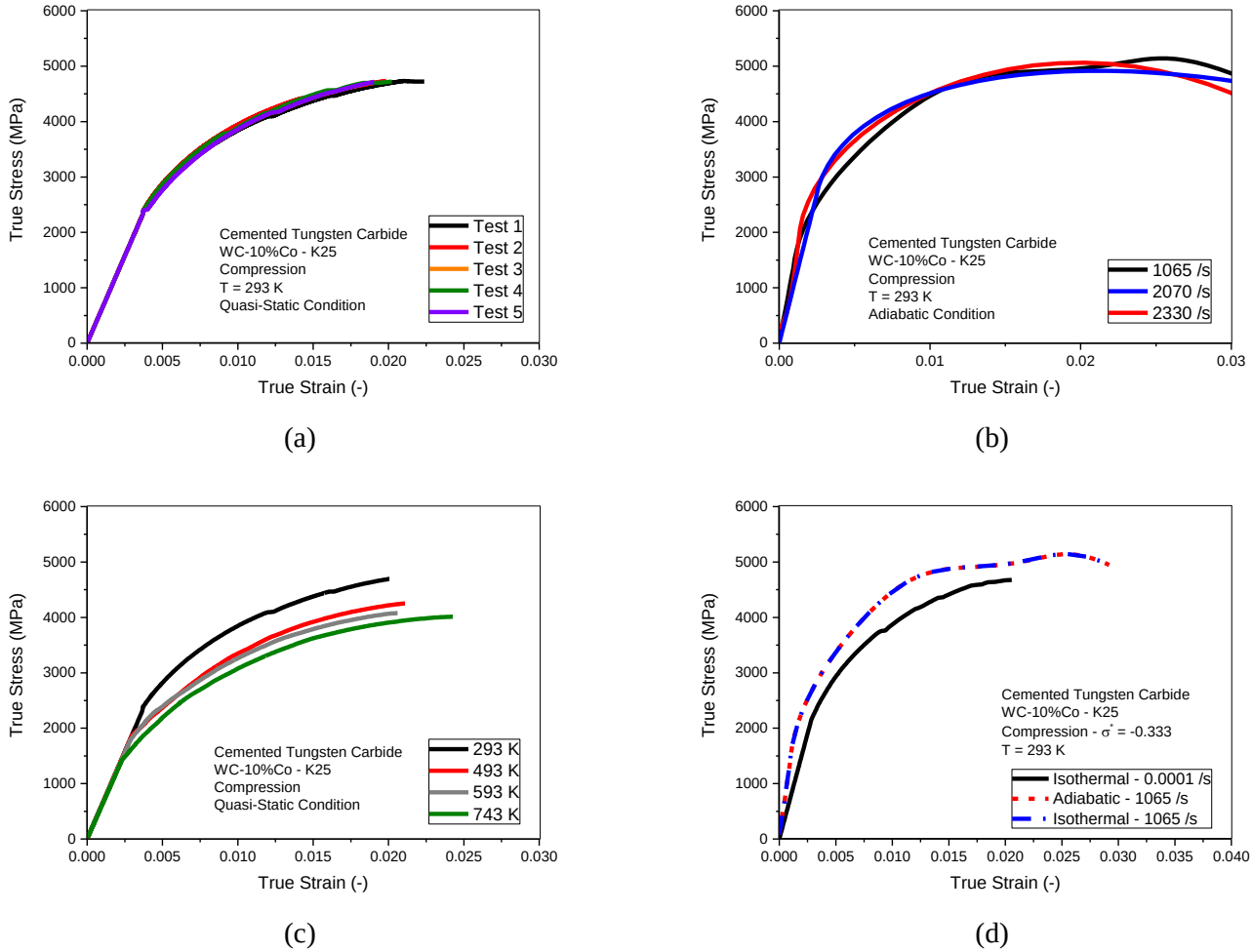

Figure 3 - True strain vs true stress curves in compression for (a) quasi-static and (b) dynamic conditions, (c) at elevated temperatures. (d) is a comparison between quasi-static and dynamic conditions

Only quasi-brittle behavior has been observed with fragmentation of the samples. The value of the plastic strain at failure seems to slightly increases with both temperature and strain rate. Some SEM fracture profiles can be observed in Figures 4.a and b at two different magnifications. On Figure 4.a, some grooves can be observed. They show the direction of propagation of the crack during the failure in the WC ceramic matrix. The metallic phase of HCP cobalt is has partially melted at the surface of the facture profile as it can be seen more in details on the Figure 4.b. The failure occurred inside the ceramic WC matrix. This last is caused by the propagation of dislocations in Co grains on the grain boundaries with WC grains and slip spreads the WC grains in the vicinity of cobalt [11]. Slip transfers across favorably oriented WC-WC boundaries leading to the creation of intergranular cracks due to immediate plastic incompatibility. Some additional slip systems in the WC grains leads to transgranular cracks [11]. The relative ductility of the material, given by the metallic cobalt phase allowing the limited but present structural hardening, seems to allow a relative low dispersion on the values of the plastic strain at failure in compression condition (around 4%).

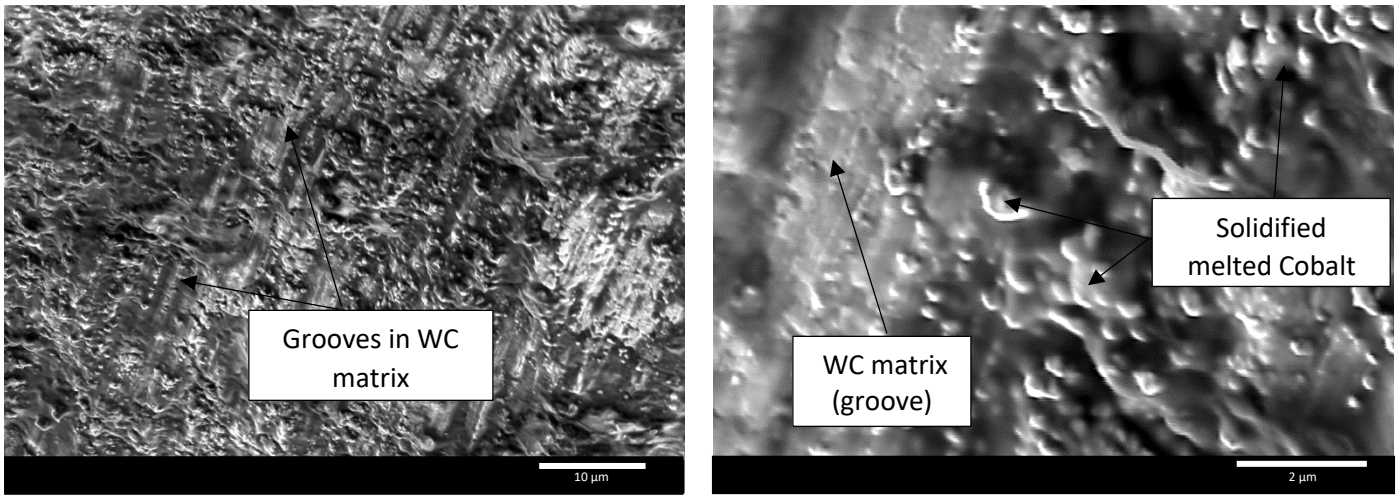

(a) (b)

Figure 4 - SEM pictures of fracture profiles in compression conditions at the following magnifications: (a) x2000 and (b) x12000

b. Shear-compression condition

The raw data of load and specimen shortening in quasi-static and dynamic conditions have been processed to obtain the true equivalent strain-true equivalent stress curves respectively in the Figures 5.a and b. As for the compression condition, the reproducibility of the results allows the validation of experimental procedure. A strain rate sensitivity of the stress is observable between the quasi-static and dynamic cases (see Figure 5.c).

It can be observed that the strain hardening is radically different in shear-compression than in compression. Indeed, a quasi-linear hardening is reported in the shear-compression case. The hardening rate is also much lower in shear-compression than for compression (Figure 5.d). Moreover, the equivalent strain at failure is twice more in this last case than in compression. These effects might be caused by the activation of different slip systems than for the compression case, causing a different hardening history and as well as a different behavior to failure [11].

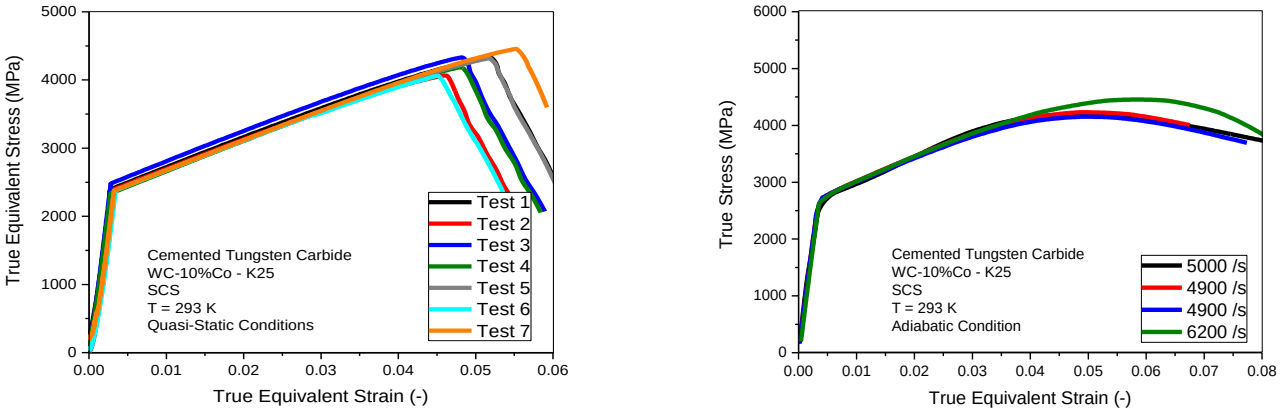

(a) (b)

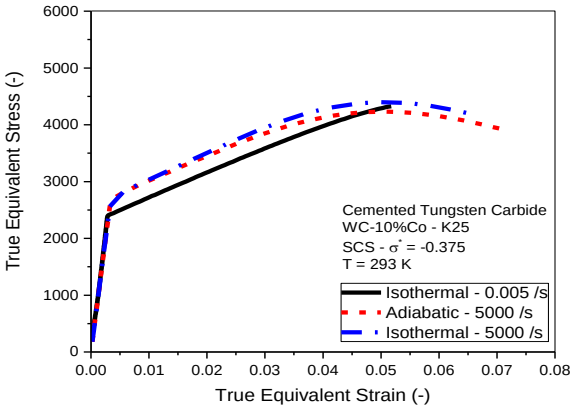

(c)

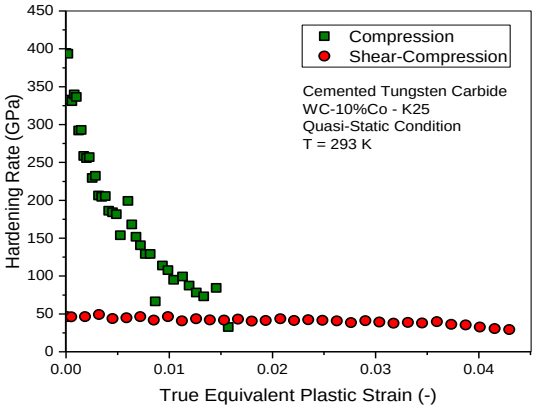

(d)

Figure 5 - True equivalent strain vs true equivalent stress curves in shear-compression for (a) quasi-static and (b) dynamic conditions, (c) a comparison between quasi-static and dynamic conditions and (d) a comparison of the hardening rate between compression and shear-compression state of stress

Concerning the failure behavior, it always occurred inside the groove of the shear-compression sample. Some SEM fracture profile can be observed in Figure 6 at two different magnification (same as for compression pictures). In this case, it can be seen that the ceramic WC matrix (in bright) has been sheared under the low local pressure leading to a clear fracture profile with very few reliefs at its surface (Figure 6.a). The metallic cobalt matrix can also be observed (darker phase) and is partially melted as in the compression case. Figure 6.b shows the details of a sheared edge of the WC ceramic matrix. In all cases, the failure is very brittle with nearly instantaneous damage propagation (cracks) along the groove of the shear-compression sample. As for the compression case, the relative ductility of the material seems to allow a relative low dispersion (6.6%) on the values of the plastic strain at failure in compression condition. The different activated slips systems and the higher isostatic pressure leads to a different behavior to the failure of the material [11].

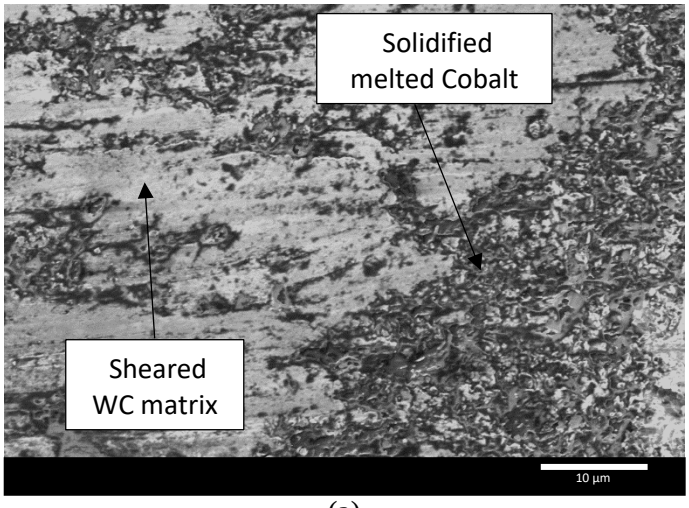

(a)

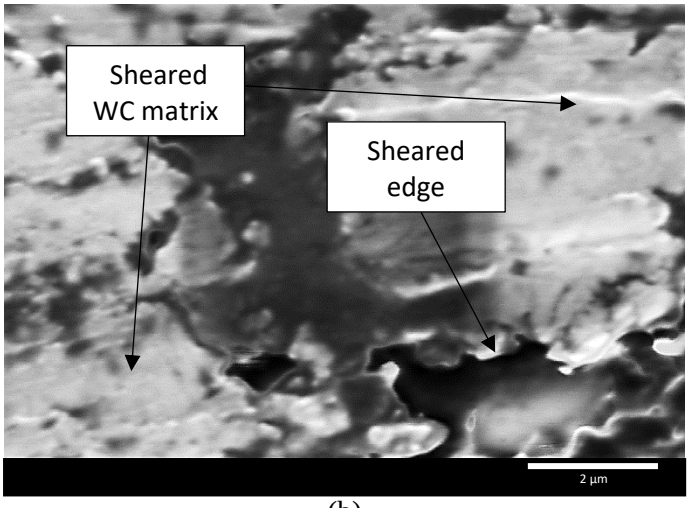

(b)

Figure 6 - SEM pictures of fracture profiles in shear-compression conditions at the following magnifications: (a) x2000 and (b) x12000

5. Constitutive modeling of stress flow

The experimental data gathered in compression allows the determination of the material parameters of the Johnson-Cook model for the stress σ presenting dependencies to the plastic strain ε_p, the plastic strain rate $\dot{\varepsilon}_p$ and the temperature T. Other analytical models can be considered (Zerilli-Armstrong [17],

MTS [18], Rusinek-Klepaczko [19] or CCH models [20]) but the Johnson-Cook model [9] is the most used in the industry and is adapted to such hardening profile.

$$\sigma(\varepsilon_p, \dot{\varepsilon}_p, T) = \left(A + B{\varepsilon_p}^n\right)\left(1 + C\ln\left(\frac{\dot{\varepsilon}_p}{\dot{\varepsilon}_{01}}\right)\right)\left(1 - \left(\frac{T - T_r}{T_m - T_r}\right)^m\right) \quad (5)$$

With A, B, n, C and m model parameters, T_m the melting temperature of the material, T_r and $\dot{\varepsilon}_{01}$ are respectively the reference temperature and strain rate at which the parameters A, B and n have been calibrated. All the parameters of the model are gathered in Table 3.

It can be observed on Figure 7.a that the strain rate sensitivity of the stress (determined at $\varepsilon_p = 0.01$) is quite limited between quasi-static and dynamic conditions but still not negligible. It can be noted that the strain rate sensitivity seems to stay the same in both tested conditions. Concerning the temperature sensitivity (Figure 7.b), even if the melting temperature is way above the tested temperature ($T_m \approx 3081\ K$), the thermal softening of the material is quite important with a decrease of 20% of the stress at 743 K (around 24% of T_m). The structural hardening of the WC-10%Co can be observed on the Figure 7.c. The structural hardening of the WC-10%Co is caused by the propagation and multiplication of the dislocations inside the HCP Cobalt binding [5, 11]. Indeed, the WC matrix is an orthorhombic ceramic which breaks at the slip activation [11]. The Johnson-Cook model suggests a sufficient modeling of its behavior due to its low plastic strain range. However, it can be seen that the structural hardening does not follow the classic isotropic hardening (modeled using power law) like many other HCP materials [21] (Mg [22] or Ti [23] based alloys). This is due to the insufficient slip systems of HCP metals (maximum 3 slip systems) for stress homogeneity assumption [21, 24] (at least 5 required) and to the resulting twinning to accommodate to the increasing strain of the grains [21, 25]. The modeling of the overall stress behavior can be seen in the Figure 7.d. The suggested Johnson-Cook model presents an efficiency sufficient for industrial application even if small loss of accuracy can be noted at low strain and high temperature. This might be due to the fact that the Cobalt phase undergoes a phase transformation from HCP to FCC lattice structures above 690 K [5] as it can be seen on Figure 7.b. This phenomenon may have a non-negligible impact the structural hardening of the material.

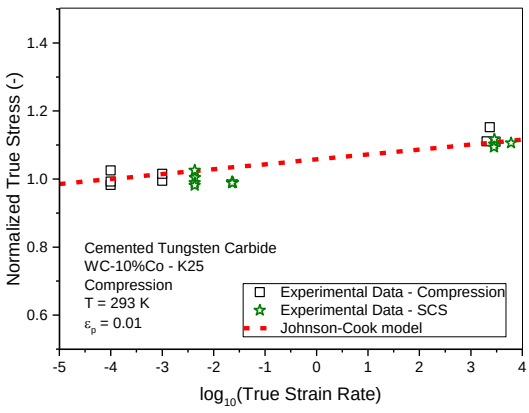

(a)

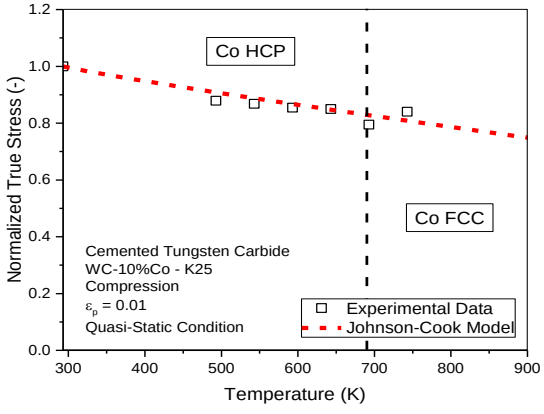

(b)

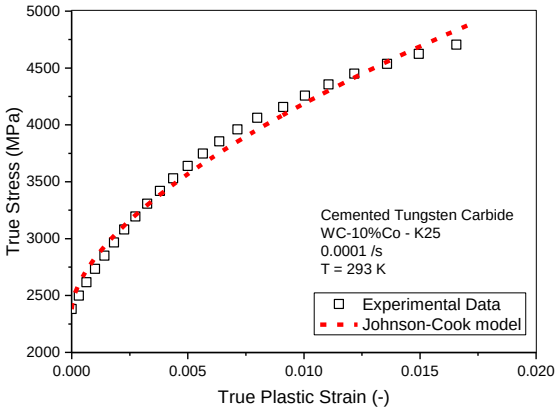

(c)

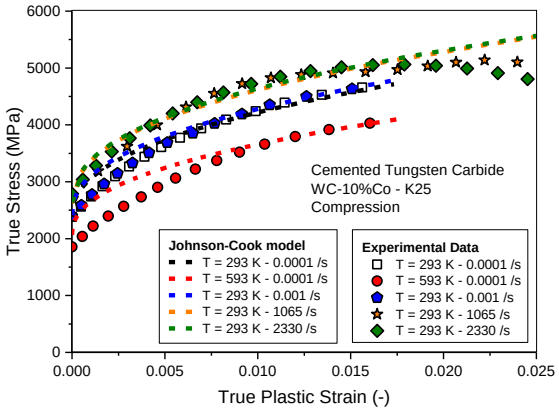

(d)

Figure 7 - The different dependencies of the stress are represented and modeled in (a) for the strain rate, (b) for the temperature and (c) for the plastic strain. (d) is the modeling of the overall stress at different temperatures and strain rates

Table 3 - Parameters of the Johnson-Cook model for the stress

A (MPa)	B (MPa)	n (-)	C (-)
2380	13580	0.4342	0.006278
m (-)	T_r (K)	T_m (K)	$\dot{\varepsilon}_{01}$ (/s)
0.9064	293	3081	0.0001

6. Conclusion

In this study, the mechanical behavior of a K25 tungsten carbide (WC-10%Co) has been investigated over a wide range of strain rates (from 0.0001 /s to 6000 /s) and from room temperature to 743 K in compression and shear-compression states of stress. The strain rate sensitivity of the metallic cobalt phase leads to an increase of the overall stress of around 10% over the range of tested strain rates. The temperature sensitivity has revealed a softening of the material of around 20% between 293 K (room temperature) and 743 K. The increase of the plastic strain at failure due to the strain rate and to the elevation of the temperature are both around 25% (over the same ranges than for the stress). However, nonlinear behaviors with the temperature due to the phase transformation of the Cobalt phase from HCP to FCC structure at 690 K are observed for both stress and plastic strain at failure.

All the experimental data have then been used to determine the parameters of the Johnson-Cook models for stress flow. The modeling using the Johnson-Cook for the stress behavior provides a sufficient accuracy for the tested conditions due to the low level of plastic strain before failure in compression. However, the hardened phase being HCP, the mechanical response of the tested material might present some change due under different types of loading like it has been shown for the shear-compression condition in this study. Indeed, the difference of the hardening rates of compression and shear-compression allows to assume that the main activated hardening mechanisms are not the same. To understand the nature of such mechanisms, additional experimental tests and microstructural investigations on the activation of twinning or of the different slip systems for different type of loading mode (e.g. shear or tensile) might be required.

The failure behavior can also be investigated further by performing tests at higher triaxialities such as shear and tension states to complete the shear-compression data obtained in this study. A Johnson-Cook model for failure [10] (or another model) could then be calibrated.

7. References

1. Jianxin, D., et al., *Friction and wear behaviors of WC/Co cemented carbide tool materials with different WC grain sizes at temperatures up to 600 C.* International Journal of Refractory Metals and Hard Materials, 2012. **31**: p. 196-204.
2. Fang, Z.Z., et al., *Synthesis, sintering, and mechanical properties of nanocrystalline cemented tungsten carbide–a review.* International Journal of Refractory Metals and Hard Materials, 2009. **27**(2): p. 288-299.
3. Acchar, W., et al., *Strength degradation of a tungsten carbide-cobalt composite at elevated temperatures.* Materials Characterization, 1999. **43**(1): p. 27-32.
4. Ferreira, J., et al., *A study on the mechanical behaviour of WC/Co hardmetals.* International Journal of Refractory Metals and Hard Materials, 2009. **27**(1): p. 1-8.
5. Exner, H. and J. Gurland, *A review of parameters influencing some mechanical properties of tungsten carbide–cobalt alloys.* Powder metallurgy, 1970. **13**(25): p. 13-31.
6. Cha, S.I., S.H. Hong, and B.K. Kim, *Spark plasma sintering behavior of nanocrystalline WC–10Co cemented carbide powders.* Materials Science and Engineering: A, 2003. **351**(1): p. 31-38.
7. Kenny, P., *The application of fracture mechanics to cemented tungsten carbides.* Powder metallurgy, 1971. **14**(27): p. 22-38.
8. Östberg, G., et al., *Mechanisms of plastic deformation of WC–Co and Ti (C, N)–WC–Co.* International Journal of Refractory Metals and Hard Materials, 2006. **24**(1): p. 135-144.
9. Johnson, G.R. and W.H. Cook. *A constitutive model and data for metals subjected to large strains, high strain rates and high temperatures*. in *Proceedings of the 7th International Symposium on Ballistics*. 1983. The Netherlands.
10. Johnson, G.R. and W.H. Cook, *Fracture characteristics of three metals subjected to various strains, strain rates, temperatures and pressures.* Engineering fracture mechanics, 1985. **21**(1): p. 31-48.
11. Rowcliffe, D.J., et al., *Compressive deformation and fracture in WC materials.* Materials Science and Engineering: A, 1988. **105**: p. 299-303.
12. Dorogoy, A., D. Rittel, and A. Godinger, *Modification of the shear-compression specimen for large strain testing.* Experimental mechanics, 2015. **55**(9): p. 1627-1639.
13. Jankowiak, T., A. Rusinek, and T. Lodygowski, *Validation of the Klepaczko–Malinowski model for friction correction and recommendations on Split Hopkinson Pressure Bar.* Finite Elements in Analysis and Design, 2011. **47**(10): p. 1191-1208.
14. G.Gary, *Testing with bars from dynamic to quasi-static.* 2011.
15. Safa, K. and G. Gary, *Displacement correction for punching at a dynamically loaded bar end.* International Journal of Impact Engineering, 2010. **37**(4): p. 371-384.
16. Rollett, A.D. and U. Kocks. *A review of the stages of work hardening*. in *Solid State Phenomena*. 1993. Trans Tech Publ.
17. Zerilli, F.J. and R.W. Armstrong. *Constitutive relations for the plastic deformation of metals*. in *High-pressure science and technology—1993*. 1994. AIP Publishing.
18. Follansbee, P. and U. Kocks, *A constitutive description of the deformation of copper based on the use of the mechanical threshold stress as an internal state variable.* Acta Metallurgica, 1988. **36**(1): p. 81-93.
19. Rusinek, A. and J.R. Klepaczko, *Shear testing of a sheet steel at wide range of strain rates and a constitutive relation with strain-rate and temperature dependence of the flow stress.* International Journal of Plasticity, 2001. **17**(1): p. 87-115.
20. Francart, C., et al., *Application of the Crystallo-Calorific Hardening approach to the constitutive modeling of the dynamic yield behavior of various metals with different crystalline structures.* International Journal of Impact Engineering, 2017.
21. Yoo, M., *Slip, twinning, and fracture in hexagonal close-packed metals.* Metallurgical Transactions A, 1981. **12**(3): p. 409-418.

22. Pérez-Castellanos, J., et al., *Temperature increment during quasi-static compression tests using Mg metallic alloys.* Materials & Design, 2010. **31**(7): p. 3259-3269.
23. Nemat-Nasser, S., et al., *Dynamic response of conventional and hot isostatically pressed Ti–6Al–4V alloys: experiments and modeling.* Mechanics of Materials, 2001. **33**(8): p. 425-439.
24. Parks, D.M. and S. Ahzi, *Polycrystalline plastic deformation and texture evolution for crystals lacking five independent slip systems.* Journal of the Mechanics and Physics of Solids, 1990. **38**(5): p. 701-724.
25. Davis, K. and E. Teghtsoonian, *Deformation twins in cobalt.* Acta Metallurgica, 1962. **10**(12): p. 1189-1191.